ADVANCED FUNCTIONAL MATERIALS
www.afm-journal.de

Kitchen Chemistry 101: Multigram Production of High Quality Biographene in a Blender with Edible Proteins

*Ajith Pattammattel and Challa Vijaya Kumar**

A high yielding aqueous phase exfoliation of graphite to high quality graphene using edible proteins and kitchen chemistry is reported here. Bovine serum albumin (BSA), β-lactoglobulin, ovalbumin, lysozyme, and hemoglobin are used to exfoliate graphite and the exfoliation efficiency depended on the sign and magnitude of the protein charge. BSA showed maximum exfoliation rate, facilitated graphite exfoliation in water, at room temperature, by turbulence/shear force generated in a kitchen blender at exfoliation efficiencies exceeding 4 mg mL^{-1} h^{-1}. Raman spectroscopy and transmission electron microscopy indicated 3–5 layer, defect-free graphene of 0.5 µm size. Graphene dispersions loaded on a cellulose paper (650 µg cm^{-2}) showed the film conductivity of 32 000 S m^{-1}, which is much higher than graphene/polymer composites. Our method yielded ≈7 mg mL^{-1}, BSA-coated graphene with controllable surface charge, which is stable under wide ranges of pH (3.0–11) and temperature (5.0–50 °C), and in fetal bovine serum, for more than two months.These findings may lead to the large scale production of graphene for biological applications.

1. Introduction

A facile route for the large scale production of water dispersible, few layer graphene (FLG) by shear exfoliation of graphite using inexpensive, edible proteins is reported. Applications of graphene in the biomedical and healthcare sectors require hydrophilic and biocompatible graphene derivatives.[1] Graphene oxide (GO) is often used as a precursor of graphene, but its potential is limited by oxidative defects and toxic metallic impurities introduced during the synthesis and exfoliation process.[2] Although the successful exfoliation of graphite to pristine graphene using organic solvents,[3,4] ionic liquids,[5,6] or surfactants[7] has been reported, the biocompatibility of the resulting product, quality, expense, and environmental impact of the production methods still remain unaddressed.[8]

Ultrasonication was used to exfoliate graphene with biological agents such as bovine serum albumin (BSA).[9–11] These proteins are suggested to adsorb to graphite platelets and facilitate delamination upon ultrasonication.[9–11] The adsorbed protein might inhibit restacking of the graphene sheets and could contribute to nanoplate stability.[11] However, sonication was suggested to introduce oxidative defects (O = 10%–25%),[12] particularly if the parent graphene has defects and the scalability of this process is particularly challenging and only low exfoliation efficiencies have been reported earlier (<1 mg mL^{-1} h^{-1}).[13]

Recently, shear force/turbulence methods were used in a kitchen blender for the mechanical exfoliation of graphite at rapid exfoliation rates.[13–15] This method offers low oxidative damage (O > 5%)[15] and in high yields. This approach was mainly used with organic solvents, *N*-methyl pyrolidine (NMP),[13] dimethyl formamide (DMF),[15] and some surfactants.[14] The shear produced and the turbulent flow exceeds the critical Reynolds number required for delamination (10^4),[15] and even a simple kitchen blender was shown to be a feasible apparatus for graphene production.[14,15]

Herein, we report shear-exfoliation of graphite in a kitchen blender with edible proteins to produce high concentrations of nearly defect-free graphene aqueous dispersions in less than an hour (**Scheme 1**). By combining the advantages of the protein's characteristics as an exfoliating/stabilizing agent for graphene and the feasibility of the shear exfoliation, high quality graphene is produced rapidly. The proteins we tested for exfoliation efficiency includes, bovine serum albumin (BSA), β-lactoglobulin, ovalbumin, lysozyme, and hemoglobin, which are inexpensive, edible proteins, and they are either waste products form the meat industry or from egg and milk.[16] The surface charge of the protein played a critical role in the exfoliation and stabilization of graphene dispersions. Our protein based shear/turbulence exfoliation is favorable over sonication or organic solvent methods in terms of yield, quality and water dispersion properties. Our results are described below.

2. Results

A facile method for producing unoxidized, pristine graphene under biologically benign conditions is essential for widespread biomedical applications of graphene. Rate of exfoliation, scalability, high quality, controlled functionalization, size and large flake size are highly desired. Rapid production of biofunctionalized, micrometer size, and defect free, few layer graphene (FLG) is reported here. Further, we have systematically examined

A. Pattammattel, Prof. C. V. Kumar
Department of Chemistry
Department of Molecular and Cell Biology
and the Institute of Material Science
University of Connecticut
55 North Eagleville Road, Unit 3060
Storrs, CT 06269-3060, USA
E-mail: Challa.Kumar@uconn.edu

DOI: 10.1002/adfm.201503247

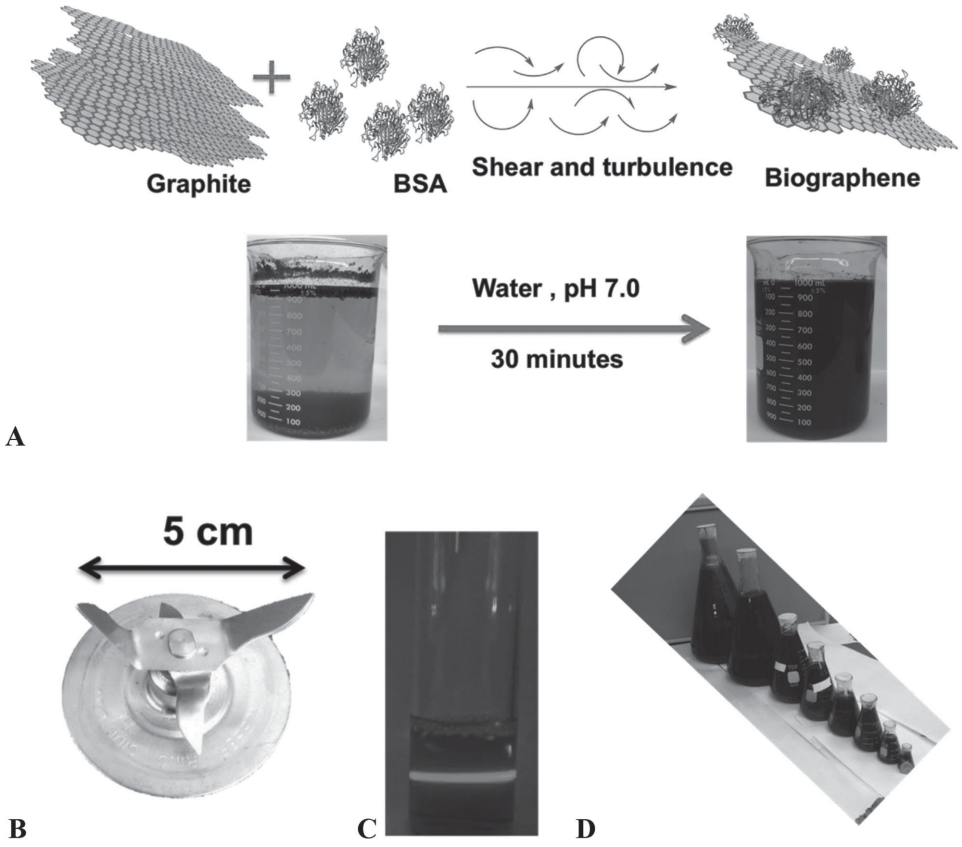

Scheme 1. A) Shear exfoliation of graphite using bovine serum albumin (BSA) in water at pH 7.0. B) Type of blades used to generate the turbulence and shear. C) Visualization of graphene formation by laser light scattering. D) Scalability of the method is demonstrated where the largest conical flask is 8 L.

particular experimental variables on the exfoliation process. Our data show that protein charge, both magnitude and sign, are critical for efficient exfoliation of graphite. The samples are extensively characterized and have record high conductance and stability in aqueous media.

2.1. Graphite Exfoliation with Protein Solutions

A suspension of graphite crystals ([Graphite] = 100 mg mL^{-1}) in 200 mL deionized (DI) water at pH 7.0 containing the protein (3.0 mg mL^{-1}) was subjected to shear in a kitchen blender for 30 min. Samples were taken every 5 min to examine the rate of exfoliation and blending was stopped to avoid overheating (<30 °C). The extinction at 660 nm (E_{660}) of the suspension was used to quantify the graphene concentrations, after removing the unexfoliated graphite, separated by centrifugation at 1500 rpm for 45 min. The extinction coefficient of BSA modified graphene was 398 mL mg^{-1} m^{-1} which was calculated using the calibration plot (Figure S1, Supporting Information).

2.1.1. Effect of the Nature of the Protein on Exfoliation

The proteins used in this study to exfoliate graphite were cheap and found in food sources to ensure the biocompatibility of the produced graphene. BSA (bovine serum), β-lactoglobulin (bovine milk), lysozyme (egg white), ovalbumin (egg white), and hemoglobin (bovine blood) were used to prove the hypothesis that proteins are effective tools for biological production of graphene in water. Four of these five proteins exfoliated graphite, but the exfoliation efficiency strongly depended on protein charge,[10] with BSA giving the highest efficiency (**Figure 1**, and Figure S2, Supporting Information). Graphene production is directly correlated with the extent of negative charge of the protein used. Therefore, we choose BSA as the model system and systematically evaluated how particular experimental parameters influence the exfoliation rate.

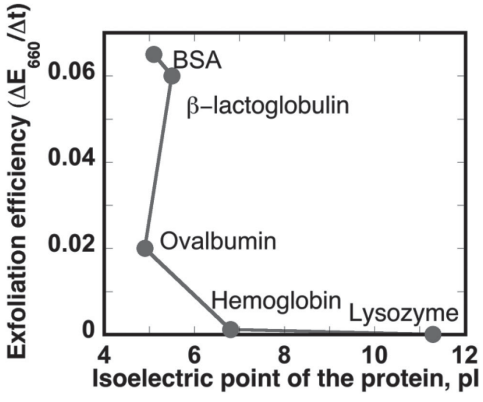

Figure 1. Plot showing the efficiency of proteins to exfoliate graphite at neutral pH is correlated with the isoelectric points (pI) of the proteins.

2.1.2. BSA Concentration Dependence

The rate of graphene production (mg h^{-1}), at constant blade speed of 17 krpm, is plotted against $[BSA]_o$ in **Figure 2**A. As the $[BSA]_o$ increased from 0.50 to 3.0 mg mL^{-1} and an increase in rate was observed from 400 to 725 mg h^{-1} which corresponds to ≈4 mg mL^{-1} h^{-1} efficiency of exfoliation. Above 3.0 mg mL^{-1} [BSA], no significant increase in exfoliation rate was observed and this concentration was used to optimize the graphite concentration for exfoliation.

2.1.3. Effect of Graphite Concentration

The graphite concentration was suggested to affect graphene production rate, due to collisions between the crystallites which can assist in exfoliation. Experiments, therefore, were conducted using 20, 40, 60, 80 and 100 mg mL^{-1} $[Graphite]_o$ and fixed $[BSA]_o$ (3.0 mg mL^{-1}) in 200 mL DI water at pH 7.0. Exfoliation rate at 17 krpm blade speed was linearly correlated with exfoliation rate as shown in Figure 2B. The slope of the line displays an increase in the production rate by 6.8 mg h^{-1} per mg mL^{-1} of graphite. Starting with high graphite concentration is not challenging because of its low cost, abundance and recyclability but gaining high efficiencies are advantageous for large scale production of graphene, as demonstrated here.[14] Since protein binding to the solid was essential for exfoliation, next we examined the effect of graphite to BSA concentration ratio (mass/mass) on the exfoliation rate.

2.1.4. Effect of Graphite to BSA Ratio

The effect of graphite to BSA ratio on exfoliation rate was studied by measuring the exfoliation rate at 15 different ratios of graphite to BSA, ranging from 0 to 100. The ratio of BSA to graphite did not influence the exfoliation rate, above $[BSA]_o$ = 3 mg mL^{-1} but rather depends on initial concentrations ($[BSA]_o$ and $[Graphite]_o$) in the solution (Figure 2C). At lower $[BSA]_o$ (1.0 mg mL^{-1}), the ratio was more significant and the exfoliation rate sharply increased from 170 to 500 mg h^{-1} as the $[Graphite]_o$ was increased from 20 to 100 mg mL^{-1} (Figure 2B, circle). The highest exfoliation rate was observed at graphite to BSA ratio of ≈33 (mg mg^{-1}) at $[Graphite]_o$ of 3.0 mg mL^{-1} (square), where the $[Graphite]_o$ was 100 mg mL^{-1}. For the next set of the experiments, we increased the $[BSA]_o$ to 8.0 mg mL^{-1} and further increase has been observed (diamond). Next, we studied the effect of pH in exfoliation rate.

2.1.5. Effect of pH

Since the graphene stacking may be inhibited by excess charge on the platelets, we tested the influence of protein charge on exfoliation rate. One simple way to control protein charge is via pH, and we have examined the exfoliation rate at pHs 1.0, 3.0, 5.0, 7.0, and 9.0 at fixed concentration of BSA (3.0 mg mL^{-1}) and graphite (100 mg mL^{-1}), at constant volume (200 mL) and constant blade speed (17 krpm). As shown in Figure 2D, exfoliation rate is strongly dependent on pH, and neutral or alkaline pHs or most favorable. Exfoliation

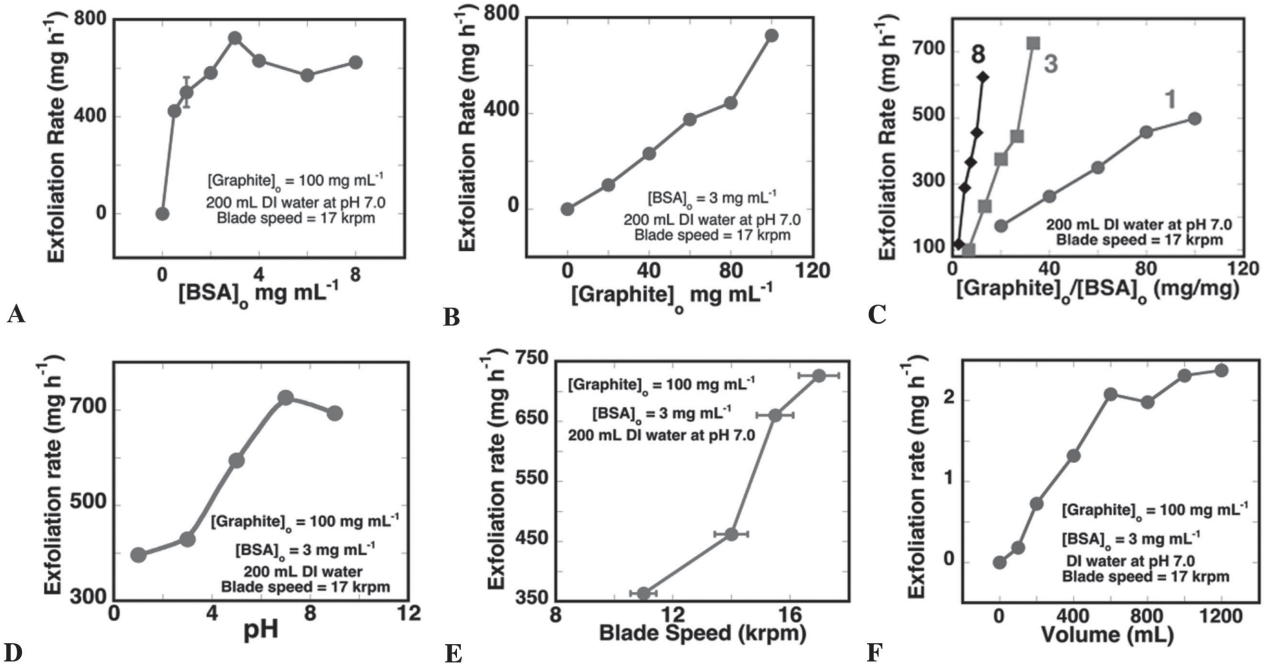

Figure 2. Rate of graphene exfoliation as a function of A) BSA concentration, B) Graphite concentration, C) Graphite to BSA concentration ratio (1, 3, and 8 represents the $[BSA]_o$ in mg mL^{-1}), D) Function of pH, E) Function of blade speed, and F) Function of volume of the suspension. Some error bars are too small to be visible.

rate increased from 375 to 725 mg h^{-1} as pH changed from 3.0 to 7.0. We suspect that increased negative charge on BSA (pI is 5.3) increases the exfoliation rate. This hypothesis was later verified by measuring the zeta potentials of biographene at various pH conditions (shown below). At pH conditions close to the pI of BSA, low zeta potential (lower than ±10 mV) was noted, representing low colloidal stability of the suspensions. Next, we examined the effect of blade speed on exfoliation because increased speed increases the shear forces on the crystallites.

2.1.6. Effect of Blade Speed

Since exfoliation is due to the shear produced in the blender, we examined how the blade speed is related to generating the critical shear force (Reynolds number = 10^4) required for exfoliation. The systematic increase in blade speed from 11 to 17 krpm, limited range in a kitchen blender, showed increased exfoliation rate from 375 to 725 mg h^{-1} (Figure 2E). A linear fit of the plot suggests 65 mg h^{-1} per krpm increase blade speed, which is significant. Further increase in speed is limited by the available options in a kitchen blender. In addition to the blade speed, the volume of the suspension also contributes to the shear rate, which is examined next.

2.1.7. Effect of Volume

The change in volume of the exfoliation addresses two potentially important questions: 1) Is the method scalable by increasing the suspension volume and, 2) how the shear rate is influenced by the volume. The data show that as the volume increased from 100 to 1200 mL, the production rate increased monotonously (Figure 2F). At a maximum volume possible in a common kitchen blender (1.2 L), a high rate of 2.4 g h^{-1} was observed. This demonstrates the possibility for gram-scale production of graphene by this approach. The increase in volume, however, resulted in decreasing the effective exfoliation efficiency from 3.7 (at 200 mL) to 2.0 mg mL^{-1} h^{-1}, at the maximum volume of 1200 mL (Figure S3, Supporting Information). This can be seen as a consequence of the decrease in effective shear rate because of the increase in volume.[14]

2.2. Characterization of Graphene Suspensions

The quality of graphene produced is analyzed using Raman spectroscopy, transmission electron microscopy (TEM), scanning electron microscopy (SEM), and colloidal stability studies.

2.2.1. Raman Spectroscopy

Raman spectroscopy has been extensively used as a versatile tool for the characterization of graphene.[17] Exfoliation of graphite to graphene, and the quality of the dispersion was assessed by Raman spectroscopy of dried graphene films on a glass surface. Typical Raman spectra of graphene (**Figure 3**A, solid lines) showed G (≈1585 cm^{-1}), D (≈1350 cm^{-1}), and 2D (2705 cm^{-1}) bands, with significant differences in intensity and shape, compared to the parent graphite flakes (dotted lines). The signature of 2D band was very prominent in the exfoliated samples, i.e., a broader (FWHM ≈ 75 cm^{-1}) and symmetric peak was appeared, in contrast to unsymmetrical peak of graphite.[17]

The apparent changes in intensity of Raman peaks give an idea about the size, defect, and number of layers present in the exfoliated graphene.[13] Remarkably, the increase in intensity of D band, which quantitatively represents disorders and edge carbon atoms, has increased after the exfoliation. An increase in I_D/I_G ratio from ≈0.1 to ≈0.6 is observed after 30 min of exfoliation. Another noticeable change was the appearance of the shoulder peak the G band called D' band, which is activated by defects.[17] The increase in intensity of 2D band resulted in $I_{2D}/I_G \approx 0.9$ qualitatively represents the presence of FLG in the suspension. Further, a statistical analysis of number of layers (N_G), lateral size ($\langle L \rangle$) and type of defects in our samples was examined using the Raman intensity ratios (Figure 3C,D).[13]

The statistical analysis was perfomed using Equations (1) and (2), from the intensity ratios of six different spectra. The number of layers in the graphene was calculated using the ratio

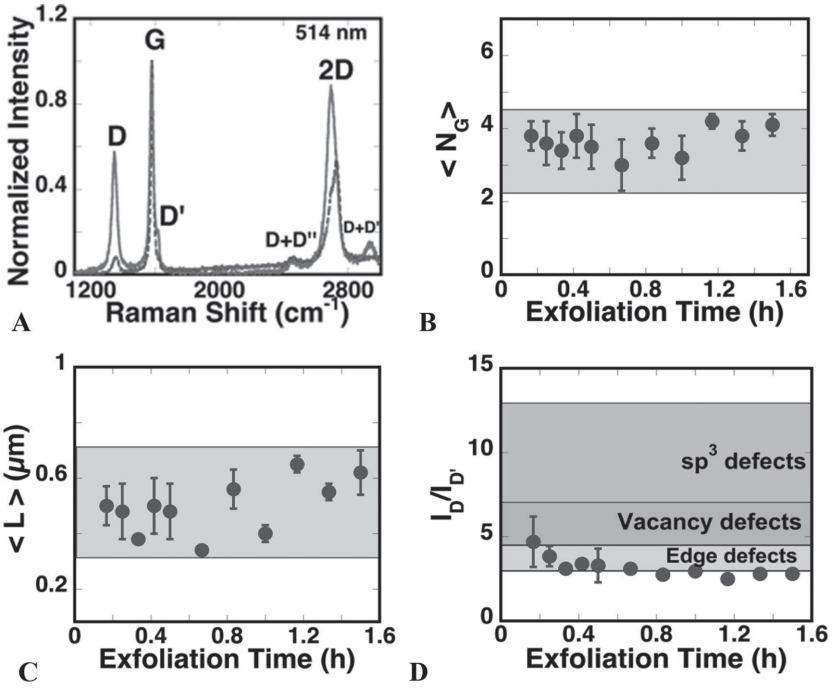

Figure 3. A) Raman spectra of graphene (blue) in comparison with graphite (red). B) Change in number layers in graphene with exfoliation time, as calculated using Equation (3). C) Change in lateral size of graphene sheets with exfoliation time, as calculated using Equation (3). D) Raman analysis of graphene showing minor edge defects. All the analysis were done using six Raman spectral data sets per sample.

of I_{2D} to its shoulder peak (I_{2D} = 30 cm^{-1}), which is prominent only in the graphite spectrum (Figure 3A, red lines). The above ratio in the graphene samples was noramlized with the ratio of precursor graphite, according to the published empirical formula.[13] The analysis gave N_G as 3.6 (±0.4) in the samples, regardless of the exfoliation period (Figure 2B). It is noteworthy that the Raman spectra are done in dried, precipitated samples, so the cacluated value would be overestimated, and suggested to be substantiated using microscopy studies.[11,13,17]

The lateral size of exfoliated graphene is calculated from I_D/I_G ratios, using Equation (3)[13] as a function of exfoliation time. The average size of the sheets was 0.5 (±0.1) μm and appeared to be highly uniform (Figure 3C). This suggests that the delamination and fragmentation of the platelets are happening simultaneously at the intial stages of exfoliation process. To futher validate the exfoliation mechanism the FLG was subjected to blending for 90 min. The blending of biofunctionalized FLG was tested for fragmentation and delamination using Raman spectroscopy (Figure S4, Supporting Information). The findings suggest that there is no further delamination or fragmentation was occurred at this step. This supports the recent kinetic theory on exfoliation of 2D materials that the exfoliation is driven by the delamination multilayared graphite and further exfoliation of FLG is kinetically unfavorable.[18]

The ratio of I_D to $I_{D'}$ represents the type of defect(s) present in the graphene.[13] The maginitude of $I_D/I_{D'}$ in our samples was 3.2 (±0.6), which is within the range of edge type defects (Figure 3D). It is very important to note that we do not have any major sp^3 defects, which suggests that no oxidation to the sheets was noticed during the exfoliation process. As such, the Raman studies clearly endorse the successful exfoliation of graphite to few layer, micrometer size and defect free graphene. The findings from Raman studies were further verified using microscopy studies as follows.

2.2.2. Microscopy Studies

TEM images were used to distinguish the number of layers present in the solution, which confirms the degree of exfoliation. TEM images were collected using dried, deposited graphene (20 μg mL^{-1}) on a Cu-grid (**Figure 4**A–D) and compared with the SEM image of graphite (Figure S5, Supporting Information). Representative images shown in Figure 4 suggest the presense of few layers of stacked graphene sheets with micrometer lateral size. The histogram of the sheet size measured from 10 to 15 sheets using diffrerent TEM images is given in Figure 4F, shows a broader distribution in size. The sheets are found to have a folded or crumbled morphology, which reduces the average lateral size (Figure 4A–D). This could decrease the average size of sheets measured by TEM (Figure 4F), when compared to Raman analysis (Figure 3C). A selected area electron diffrection pattern of the crumble sheet in Figure 4A is shown in Figure 4E, which implied a polycrystalline phase which could be due to the presence of amorphous BSA functionalization on the sheets and foldings. Overall, the TEM studies supported the successful exfoliation of graphite to micrometer size biofunctionalized FLG.

2.2.3. Biofunctionalization of Graphene

Production of aqueous graphene dispersions, in particular, with stability in biological conditions is an active research area in chemical and biomaterial sciences. Water stability of graphene derivatives is usually attributed to hydrophilic modification. Here, by in situ modification of graphene with BSA, we achieved graphene aqueous dispersions with concentrations as high as 6.8 mg mL^{-1}.

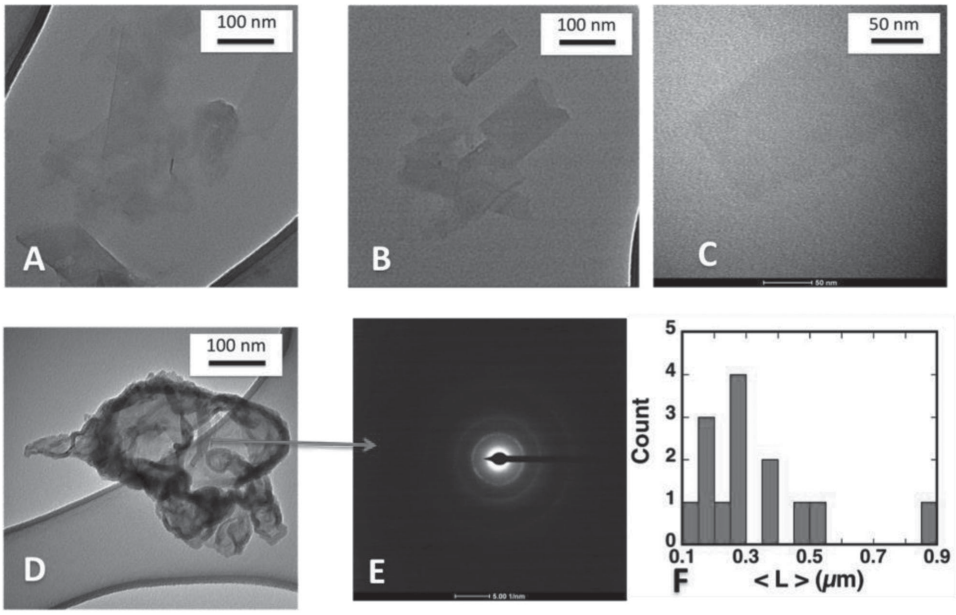

Figure 4. TEM images of graphene samples show A,C) few layer distribution in the samples, and D) Crumpled sheets. E) Selected area electron diffraction pattern of folded sheet in (D). F) Histogram showing the size distribution from TEM images (Figure S5B, Supporting Information).

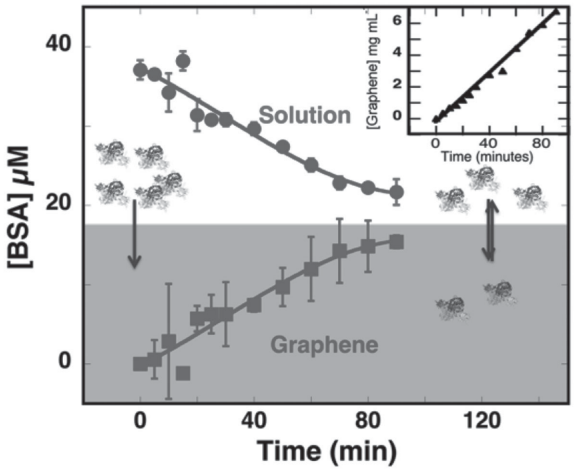

Figure 5. In situ biofunctionalization of graphene is confirmed by the exchange of BSA from the solution (circles) to the graphene (squares) with increasing exfoliation time. The increase in graphene concentration in the system is shown in the inset.

To prove the in situ biofunctionalization, the presence of bound BSA to graphene sheets is confirmed using UV spectroscopy and zeta potential studies. Due to strong graphene absorption at 200–300 nm, resolving the 280 nm absorption (A_{280}) of the bound protein was inconclusive (Figure S6, Supporting Information). Alternatively, we determined the unbound BSA concentration using A_{280} after separating the bound BSA by centrifugation (12 000 rpm for 45 min). We examined the free [BSA] as a function of the exfoliation time and from that we calculated the $[BSA]_{bound}$. We observed that the $[BSA]_{bound}$ gradually increasing (blue lines) as more graphene was produced in the medium (**Figure 5**, inset). Conversely, one can propose that BSA binding and exfoliation happen simultaneously using this treatment. Nonetheless, the exchange of BSA from solution to graphene phase proves the in situ biofunctionalization of graphene.

After 90 min of exfoliation, the $[BSA]_{bound}$ was 15×10^{-6} M which is ≈40% of $[BSA]_{int}$ and 18% (mass/mass) of total graphene concentration (6.8 mg mL^{-1}). The $[BSA]_{bound}$ corresponds to 3% area covered by BSA on graphene sheets, assuming that graphene is monolayer and BSA is completely intact in structure. However, since the graphene is few layered and BSA showed changes in secondary structure on binding to the graphene surface (from CD studies, Figure S7, Supporting Information), we propose that 15%–20% of the exposed graphene sheets are functionalized by BSA.

The biofunctionalization was further verified using time dependent zeta potential measurements shown in Figure S8 of the Supporting Information. We measured the zeta potential of graphene dispersions as the exfoliation progressed and found that the surface potential was constant around −27 (±3) mV at pH 7.0. The observed surface potential of graphene is attributed to the presence of bound BSA, since the pristine graphene has no sp^3 defects due to charged oxygen functional groups, such as in graphene oxide. This validates the hypothesis that the protein is been modified to the graphene and the negative charge of BSA is stabilizing the sheets in the aqueous media.

2.2.4. Colloidal Stability of Graphene Dispersions

The biological stability of aqueous graphene dispersions under relevant conditions, with varying temperatures and pHs, and in fetal bovine serum (FBS) is studied. Stability of graphene/GO dispersions at the aforementioned conditions depends on the type and degree of functionalization.[19] In the present study, BSA is the stabilizing agent for graphene, which can undergo structural changes in stresses such as pH and temperature.[20] Consequently, these changes can influence the stability of graphene dispersions and this has been investigated by UV–vis spectroscopy, and zeta potential studies.

Effect of Temperature: The role of temperature in the formation of aggregated graphene was studied in two different aspects. First, we studied the effect of temperature on aggregation at increasing temperatures from 25 to 80 °C by measuring the extinction at 660 nm. There was no significant change in concentration of graphene (using E_{660}) at elevated temperatures (Figure S9, Supporting Information). However, significant spectral changes in the 250 to 400 nm region, occurred after 60 °C, which is noticeably close to the denaturation temperature of BSA.[21] An increase in absorption at 660 nm is also due to the changes in graphene/BSA complex upon structural changes in BSA. Second, the storage stability of graphene at three different temperatures (5, 25, and 50 °C) in DI water at pH 7.0 was studied by measuring E_{660} at specific intervals for more than a month and there has been no aggregate formation (**Figure 6**A). The E_{660}

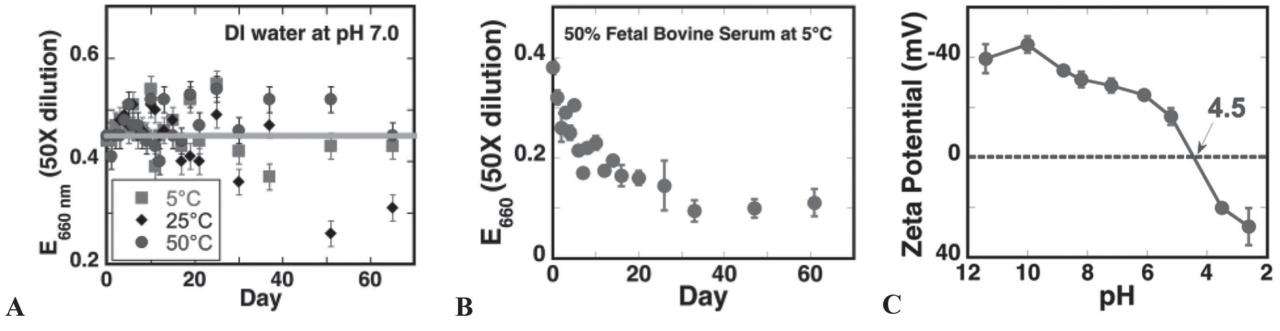

Figure 6. A) Change in graphene concentration of dispersions stored at 5, 25, and 50 °C. B) Stability of graphene in 50% fetal bovine serum (FBS). C) Zeta potentials of graphene dispersions as a function of pH.

of the graphene dispersions after 65 days showed no significant changes at 5 and 50 °C, but significant loss in concentration (≈50%) was noted for graphene stored at room temperature.

Biological uses of nanomaterials require stability in biological fluids such as serum. It is possible that graphene can bind to the biomolecules present in the serum and aggregate, which would limit its practical uses. We studied the storage stability of graphene in a 50% FBS solution at 5 °C and checked the E_{660} daily for more than two weeks. There was no detectable precipitation or aggregation when 50% FBS was added (Figure 6B) but the E_{660} showed gradual decrease (Figure 6B).

After one week, the concentration of graphene was reduced to half of its original value but retained that concentration for two more weeks with no significant drop. We hypothesize that this might be due to the activity of the proteases that are present in FBS, which might deteriorate BSA present on the graphene sheets and induce aggregation. This was confirmed by checking the stability of graphene in the presence of a protease, trypsin (0.2 mg mL^{-1}), in DI water at pH 7.4. After 1 h of incubation with trypsin at 37 °C, there was precipitation. Therefore, the protein molecule is necessary for aqueous stability of graphene sheets, which is noted by other groups as well.[10] However, the observed half-life of 10 days in FBS is relevant for biological/cellular studies of graphene. This analysis could potentially broaden the uses of our graphene in various applications, such as sensing and toxicity studies in biological fluids.

Effect of pH: The role of pH on graphene stability was studied using zeta potential measurements. Figure 6B shows the change in zeta potential (ξ) of graphene with pH, where the observed negative surface charge of graphene is due to the presence of the BSA functionalization. As the pH decreased from 11 to 2.5 the zeta potential varied from –40 to +40 mV, and the isoelectric point (ξ = 0 mV) was noted at ≈4.5 which is close to the isoelectric point of BSA.[20] Additionally, the zeta potential of graphene incubated at varying pHs was measured after incubation at 25 °C for a week. The zeta potential of the solutions was retained (≈100%) after one week (Figure S10, Supporting Information), which proves the colloidal stability of graphene dispersions over a wide range of pH (3–11). The stability was further supported by measuring E_{660} of graphene at the different pHs before and after incubation (Figure S11, Supporting Information). However, at pH value near ξ = 0 mV, aggregated graphene was formed and a substantial decrease in concentration at pH 5.1 was noted. This emphasizes the crucial role of electrostatic repulsion between protein molecules in stabilizing graphene in aqueous media. Also, this study brings out a new opportunity to design biographene with desirable pI values by using particular proteins for exfoliation.

2.2.5. Conductivity Measurements

Graphene sheets with few layers and micrometers of lateral area have high electrical conductivity.[13] The exfoliated graphene was painted onto a standard printing paper (cellulose) (22 × 14 cm, 650 μg cm^{-2}), and the conductivity has been measured using standard 4-point probe resistivity, which is more accurate than 2-point method.[22] (**Figure 7**A,B). The adsorption of graphene onto the paper was confirmed by SEM images (Figure 4C). The system showed excellent, continuous conductivity over a range from 0 to 45 V with a steady output current. The thickness of graphene layer was measured from the cross-sectional SEM image (Figure 6C) was 3 μm, which was further confirmed by theoretical calculation based on the adsorption efficiency (650 μg cm^{-2}) and density of graphite (2.2 g cm^{-3}). The sheet conductivity of the paper was calculated to be as high as 32 000 S m^{-1} using Equation (3) ($R = \rho L/Wt$) with sheet resistance (R_s) of 50 Ω sq^{-1}. High conductivity was also demonstrated in a circuit connecting a light emitting diode (LED) and a 12 V battery in Figure 7D.

3. Discussion

An efficient, simple, and robust approach for multigram production of biofunctionalized graphene from graphite, under

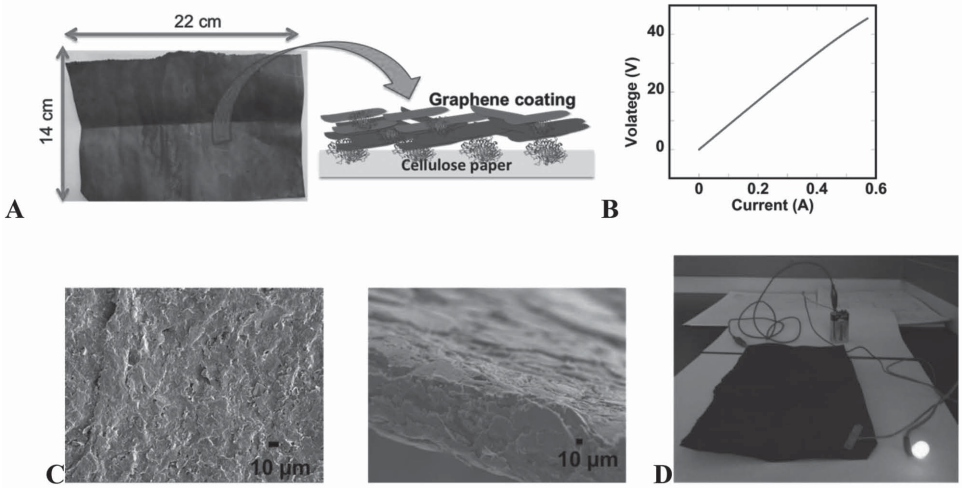

Figure 7. A) Photograph of graphene-coated paper. B) Linear *I–V* response of the paper measured using a standard 4-point circuit. C) Representative SEM images of the graphene-coated paper confirming the presence of bound graphene. D) Conductivity of the paper is illustrated by using the paper in an LED circuit.

ambient conditions, is presented here. In this top down approach, micromechanical exfoliation of graphite was achieved by the shear/turbulence in a kitchen blender and proteins were used to biofunctionalize pristine graphene sheets. The aqueous graphene suspensions show storage stability under biologically relevant conditions.

Exfoliation of graphite using biomolecules such as proteins,[9–11,23] carbohydrates,[24] and polysaccharides[25,26] offer green, biocompatible carbon-based nanomaterials for various biomedical and drug delivery applications. Recently, proteins such as BSA, lysozyme, and hydrophobins were used for liquid phase exfoliation of graphite to FLG by ultrasonication.[9–11]

Proteins are suggested to interact with graphene through hydrophobic residues but the effect of proteins in stabilizing the dispersions is yet to be established.[9] Herein, by using proteins with different surface (amino acid distribution) and bulk properties (charge and hydrophobicity), protein charge has been shown to be an important parameter for exfoliation. Not only protein adsorption on the flakes would be able to reduce the sheet-to-sheet (van der Waals) interactions, but also the charge on the protein is critical for the overall stability of the functionalized sheets. So, we noted that the proteins with sufficient surface charge (in our case > –15) showed maximum yield when compared to smaller proteins with less net charge, such as lysozyme (Figure S12, Supporting Information). Moreover, we found no correlation with other parameters such as hydrophilicity, number of charged amino acids and volume of aliphatic residues in the protein.

In general, sonication-based exfoliation was reported to have low exfoliation rates, cracking of the platelets and their oxidative damage.[12] Exfoliation rates by several methods are compared in **Figure 8**A. Sonication assisted exfoliation methods, for example, using BSA, lysozyme and hydrophobins (in 60% ethanol) demonstrated exfoliation efficiency of 0.27, 0.33, and 0.83 mg mL^{-1} h^{-1}, respectively.[9–11] Current approach achieved efficiencies of 4–7 mg mL^{-1} h^{-1} in a completely aqueous medium, and the exfoliation rate was found to be linear over an extended period of time (1.5 h, Figure S13, Supporting Information). To the best of our knowledge, this is the highest rate for liquid phase exfoliation in water (Figure 8A). The exfoliation rates were found to be affected by factors such as 1) $[BSA]_o$, 2) $[Graphite]_o$, 3) pH, 4) total volume, 5) blade speed, 6) viscosity, 8) surface tension, to name a few. Experiments with varying $[BSA]_o$ and $[Graphite]_o$ were conducted while keeping factors 3–6 constant.

Assuming that the viscosity and surface tension changes are intrinsic to protein concentrations in our experiments, the following relation for the rate of exfoliation (r) can be deduced as given in the following equation:

$$r \propto [BSA]_o^a \times [Graphite]_o^b (pH)^c (Volume)^d (bladespeed)^e$$

where *a*–*e* are the corresponding orders of the reaction. Experiments with increasing $[BSA]_o$ showed saturation of exfoliation rate at around 3 mg mL^{-1} (Figure 2A) and above this value, "*a*" is set to zero. But the rate depended more steeply and linearly on $[Graphite]_o$. This sheds light onto the mechanistic aspect of the exfoliation, in which the graphite-to-graphite collisions, with threshold Reynolds's frequency, is rate limiting in the overall exfoliation process. The bombardment causes fragmentation of the graphite platelets, which facilitates the shear exfoliation process, because of low van der Waals forces between small graphene layers.[3] In turn, BSA molecules kinetically trap the exfoliated sheets very rapidly and protect them from restacking. In addition, the other experimental variable pH, volume, protein charge, and blade speed also contributed to the exfoliation rates (Figure 2B). We fitted these data to linear plots (an approximation), and extracted the following values for our guidance: $b = 1.2$; $c = 0.29$, $d = 0.99$, and $e = 1.7$ in the above equation. Based on these, we postulate that multiple factors control the exfoliation rate, and it can be maximized in many dimensions as desired.

BSA plays three other roles in exfoliation: 1) lowering the surface tension of the medium,[33] 2) binding to the exposed graphite surface[9] and lower its surface free energy, and 3) stabilize the graphene sheets in water by positioning the charged and/or hydrophilic functional groups for favorable interactions with the solvent or enhance solvation of the platelets.[34] The intrinsic hydrophobicity of carbon nanomaterials limits their bioprocessability.[35] The availability of hydrophilic graphene is largely restricted to GO, which was shown to have structural defects, oxidative debris, and metallic impurities limiting its biological use.[36] The biofunctionalized graphene, reported here, was highly stable in water at various pHs and room temperature, which was not demonstrated in previous studies. Stability

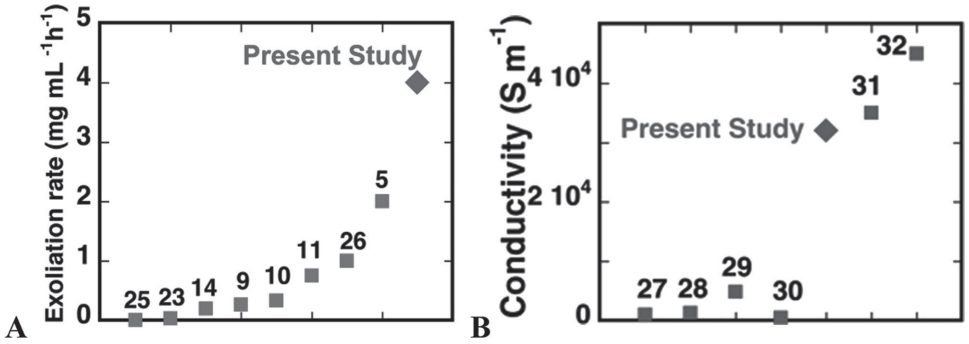

Figure 8. A) Comparison of the rate of exfoliation in aqueous media achieved in the current method with published approaches.[5,9–11,14,23,25,26] B) The high conductivity of biographene deposited on paper when compared to the conductivities of similar materials.[27–32] Reference numbers for the corresponding data are shown in each of the panels.

and in vivo and in vitro performance of nanomaterials are challenging due to aggregation, protein corona formation, and protease activity in biological fluids, particularly in serum.[37,38] Here, the biofunctionalized graphene showed initial aggregation or degradation in 50% FBS due to protease activity but no further changes occurred over several days. Biographene made here opens up new opportunities to modify its surface with many other (bio)molecules, as previously demonstrated with GO.[39]

Electrical conductivity of graphene also depends on the method of exfoliation and the degree of oxidation.[40] Surprisingly, the BSA coated graphene showed excellent sheet conductivity, which is 6–7 times better than previously reported graphene based polymeric composites (Figure 8B).[41] Values of 32 000 S m^{-1} for our biographene coated paper (22 × 14 cm) is close to the highest reported value of 45 000 S m^{-1}, in which a relatively smaller area (5 cm in diameter) was used, and the graphene was produced by GO reduction, followed by filtration.[32] Compared to these other conductive graphene papers which require laborious filtration, annealing or reduction,[27–32,42] this flexible, larger area metal-free conducting sheets indicated some of the highest values, over a large voltage window, following Ohm's law. Since many composite films show conductivities over a small voltage window (usually in mV), our sample has some advantages. The first time illustration of highly conductive graphene produced by direct exfoliation of graphite is demonstrated here with edible proteins and a kitchen blender, inexpensive apparatus without using toxic chemicals, metals or solvents.

4. Conclusions

High quality graphene suspended in aqueous media is highly desirable for the biological applications of this "wonder material." Due to its inherent hydrophobicity, graphene needs adequate biofunctionlization for its dispersion in water. Proteins were recently used as the exfoliating agents, as well as modifiers, to yield aqueous graphene dispersions via ultrasonication, which gave slow exfoliation efficiencies (<1 mg mL^{-1} h^{-1}), limited scalability (<100 mL) but induced basal plane defects, particularly with low quality graphite[12,13] Breaking of the sheets, production of reactive sites and reaction of the damaged sites with oxygen were suggested to be some of the disadvantages of sonication.[12] To overcome these disadvantages, shear/turbulence forces were used as a successful alternative, although, to date, the approach has been limited to organic media and surfactant solutions.

Here, the exciting possibilities of shear/turbulence method were coupled with the surface active properties of edible proteins and produced multigram scale synthesis of unoxidized, low-defect graphene suspensions in water. The protein charge played a key role in exfoliation of graphite, the strongly negatively charged BSA showed maximum efficiency. The GO or chemically reduced GO (rGO) used is prepared by tedious oxidation/reduction treatments; contaminate the GO with metallic or other impurities.[2] The biographene is obtained directly from graphite and proteins, which could be an alternative to GO or rGO for a variety of applications. Moreover, this approach could be extended to many other proteins, as desired for particular applications.

Herein, the graphene concentration as high as 7 mg mL^{-1} was achieved, at high rates of exfoliation, and exfoliation rate is tied with specific attributes of the reaction medium for future scale-up. An empirical relation was deduced for further optimization of the exfoliation rates. Biographene with particular isoelectric points or tunable charge can be produced by selecting appropriate proteins for the exfoliation or by controlling the pH of the medium.

These suspensions also showed long-term thermal, pH and storage stabilities under biologically relevant conditions, including in a biological fluid (fetal serum) which a very good test for biological applications. These aqueous graphene dispersions, with improved biological stability, could be good alternatives to widely used GO or rGO for a variety of applications in biomedical and bioengineering fields.[43,42] The biographene-coated cellulose paper is unique in that it is the first conductive, metal-free cellulose-protein-graphene hybrid material that has not been reported before. This simple exfoliation method could lead to greater access of graphene for laboratories with limited resources or applications that need large quantities, and it could further revolutionize the graphene field.

5. Experimental Section

Materials: Graphite crystals (≈150 μm), lysozyme (egg white), *β*-lactoglobulin (bovine milk), trypsin (bovine), and ovalbumin (egg white) were obtained from Sigma-Aldrich (St. Louis, MO). BSA and hemoglobin was purchased from Equitech-Bio Inc. (Kerrville, TX). All the proteins were used without further purification. Oster Kitchen 10 speed blender was purchased from a local shop.

Methods: Exfoliation of Graphite: All the exfoliation experiments were performed by adding calculated amounts of graphite, BSA, DI water in the kitchen blender at required blade speed. Aliquots (1 mL) of the mixture were taken every 5 min to quantify the progress of exfoliation. Samples were centrifuged at 1500 rpm for 45 min to separate unexfoliated graphite particles, and the amount of graphene in the supernatant was measured using extinction at 660 nm, using the calculated extinction coefficient of 398 mL mg^{-1} m^{-1} (Figure S2, Supporting Information). The extinction coefficient of graphene is highly dependent of the size, number of layers and functionalization present. This extinction coefficient was close to that of polysaccharide modified graphene.[26] Rate of exfoliation at different conditions of concentrations, blade speed, pH, and volume were calculated by following the exfoliation for first 20 min. All the experiments are performed in three trials, except for the optimization of the volume.

Raman Spectroscopy: Raman spectra were recorded using a 514 nm laser in Renishaw system 2000 microscope at 1 μm spatial resolution. The microscope was calibrated using typical Raman shift of Si-wafer sample at 521 cm^{-1}. Graphene samples were concentrated using centrifugation to 1 mg mL^{-1} and were dried on a Si/SiO_2 glass with ≈1 cm spot size. We observed sample destruction at 100% focused laser, probably due to the protein, so the beam was off focused by 50% during the measurement. The statistical analysis of number of layers ($\langle N_G \rangle$) from different Raman spectra was calculated using the following equation

$$\langle N_G \rangle = 10^{0.84M+0.45M^2},\ M = \frac{I_{G'ene}\left(\omega = \omega_{p,G'ite}\right)/I_{G'ene}\left(\omega = \omega_{s,G'ite}\right)}{I_{G'}\left(\omega = \omega_{p,G'ite}\right)/I_{G'}\left(\omega = \omega_{s,G'ite}\right)} \quad (1)$$

where ω_p is the 2D peak intensity and ω_s is intensity of the shoulder ($\omega_s = \omega_p$–30 cm^{-1}). The lateral size $\langle L \rangle$ of the graphene sheets was calculated using the following empirical relation

$$\langle L \rangle = \frac{k}{(I_D/I_G)_{G'ene} - (I_D/I_G)_{G'ite}} \quad (2)$$

where k = 0.17 experimentally calculated by comparing Raman intensities with microscopy data, and I_D/I_G is the ratio of D and G band intensities[13]

Microscopy Studies: TEM studies were done in a FEI Tecnai T12 using 100 kV accelerating voltage. Graphene samples (20 μg mL^{-1}) were drop casted on a Cu-grid and dried under vacuum, prior to the imaging. SEM images of graphite and graphene-coated paper were taken in a JEOL FESM 6335 using 5 kV accelerating voltage. Samples were coated with Au–Pd in Edwards E306A Coating System and directly taken for imaging.

Conductivity Measurements: Graphene suspension (4 mg mL^{-1}) was simply coated on a standard printer paper and air dried to prepare conductive graphene papers. About 200 mg of graphene was adsorbed onto a 22 × 14 cm size paper to give 650 μg cm^{-2} loading. Sheet conductivity of the paper was measured using a 4-probe measurement in a Keithley 2420 Sourcemeter, after making the contacts with Cu-tape. The *I*–*V* curve directly obtained from the instrument was used to find the resistance and the sheet resistance was calculated using the following formula,[22] where R is the resistance, ρ is the resistivity, L is the length, W is the width, and t is the film thickness measured from SEM image (Figure 7C)

$$R = \rho \frac{L}{Wt} \quad (3)$$

Zeta Potential Measurements: Aqueous graphene dispersions (1.6 mL, 0.6 mg mL^{-1}) with known pH were analyzed using the Brookhaven Zeta Plus zeta potential analyzer (Holtsville, NY). The samples were analyzed for electrophoretic mobility using laser Doppler velocimetry and, Smoluchowski fit was used to calculate the zeta potential.

Supporting Information

Supporting Information is available from the Wiley Online Library or from the author.

Acknowledgements

The authors are grateful to the University of Connecticut for financial support, and acknowledge Shailaja Gnanaguru for technical help. The authors thank Dr. Adamson for access to the conductivity apparatus.

Received: August 4, 2015
Revised: September 10, 2015
Published online: October 27, 2015

[1] C. Chung, Y. K. Kim, D. Shin, S. R. Ryoo, B. H. Hong, D.-H. Min, *Acc. Chem. Res.* **2013**, *46*, 2211.
[2] C. H. A. Wong, Z. Sofer, M. Kubešová, J. Kučera, S. Matějková, M. Pumera, *Pro. Natl. Acad. Sci. USA* **2014**, *111*, 13774.
[3] M. Yi, Z. Shen, *J. Mater. Chem. A* **2015**, *3*, 11700.
[4] X. Chen, J. F. Dobson, C. L. Raston, *Chem. Commun.* **2012**, *48*, 3703.
[5] T. Morishita, H. Okamoto, Y. Katagiri, M. Matsushita, K. Fukumori, *Chem. Commun.* **2015**, *15*, 12068.
[6] I. W. P. Chen, Y. S. Chen, N. J. Kao, C. W. Wu, Y. W. Zhang, H. T. Li, *Carbon* **2015**, *90*, 16.
[7] M. Lotya, P. J. King, U. Khan, S. De, J. N. Coleman, *ACS Nano* **2010**, *4*, 3155.
[8] K. Yang, Y. Li, X. Tan, R. Peng, Z. Liu, *Small* **2013**, *9*, 1492.
[9] S. Ahadian, M. Estili, V. J. Surya, J. Ramon-Azcon, X. Liang, H. Shiku, M. Ramalingam, T. Matsue, Y. Sakka, H. Bae, K. Nakajima, Y. Kawazoe, A. Khademhosseini, *Nanoscale* **2015**, *7*, 6436.
[10] D. Joseph, N. Tyagi, A. Ghimire, K. E. Geckeler, *R. Soc. Chem. Adv.* **2014**, *4*, 4085.
[11] A. M. Gravagnuolo, E. Morales-Narváez, S. Longobardi, E. T. da Silva, P. Giardina, A. Merkoçi, *Adv. Funct. Mater.* **2015**, *25*, 2771.
[12] T. Skaltsas, X. Ke, C. Bittencourt, N. Tagmatarchis, *J. Phys. Chem. C* **2013**, *117*, 23272.
[13] K. R. Paton, E. Varrla, C. Backes, R. J. Smith, U. Khan, A. O'Neill, C. Boland, M. Lotya, O. M. Istrate, P. King, T. Higgins, S. Barwich, P. May, P. Puczkarski, I. Ahmed, M. Moebius, H. Pettersson, E. Long, J. Coelho, S. E. O'Brien, E. K. McGuire, B. M. Sanchez, G. S. Duesberg, N. McEvoy, T. J. Pennycook, C. Downing, A. Crossley, V. Nicolosi, J. N. Coleman, *Nat. Mater.* **2014**, *13*, 624.
[14] E. Varrla, K. R. Paton, C. Backes, A. Harvey, R. J. Smith, J. McCauley, J. N. Coleman, *Nanoscale* **2014**, *6*, 11810.
[15] M. Yi, Z. Shen, *Carbon* **2014**, *78*, 622.
[16] P. H. Yun-Hwa, A. O. Jack, in *Handbook of Analysis of Edible Animal By-Products*, CRC Press, Boca Raton, Florida, USA **2011**, pp. 13–35.
[17] A. C. Ferrari, D. M. Basko, *Nat. Nanotechnol.* **2013**, *8*, 235.
[18] J. A. Texter, *Angew. Chem.* **2015**, *54*, 10258.
[19] V. Georgakilas, M. Otyepka, A. B. Bourlinos, V. Chandra, N. Kim, K. C. Kemp, P. Hobza, R. Zboril, K. S. Kim, *Chem. Rev.* **2012**, *112*, 6156.
[20] J. F. Foster, in *Albumin: Structure, Function and Uses* (Ed: V. M. R. O. A. Rothschild), Pergamon, Oxford, UK **1977**, pp. 53–84.
[21] K. Takeda, A. Wada, K. Yamamoto, Y. Moriyama, K. Aoki, *J. Protein Chem.* **1989**, *8*, 653.
[22] F. M. Smits, *Bell Syst. Technol. J.* **1958**, *34*, 711.
[23] Y. Ge, J. Wang, Z. Shi, J. Yin, *J. Mater. Chem.* **2012**, *22*, 17619.
[24] M. K. P. Kumar, S. Shanthini, C Srivastava, *R. Soc. Chem. Adv.* **2015**, *5*, 53865.
[25] V. Chabot, B. Kim, B. Sloper, C. Tzoganakis, A. Yu, *Sci. Rep.* **2013**, *3*, 1378.
[26] I. Uysal Unalan, C. Wan, S. Trabattoni, L. Piergiovanni, S. Farris, *R. Soc. Chem. Adv.* **2015**, *5*, 26482.
[27] Y. J. Yun, W. G. Hong, W. J. Kim, Y. Jun, B. H. Kim, *Adv. Mater.* **2013**, *25*, 5701.
[28] P. Šimek, Z. Sofer, O. Jankovský, D. Sedmidubský, M. Pumera, *Adv. Funct. Mater.* **2014**, *24*, 4878.
[29] Z. Xu, Y. Zhang, P. Li, C. Gao, *ACS Nano* **2012**, *6*, 7103.
[30] C. Vallés, J. David Núñez, A. M. Benito, W. K. Maser, *Carbon* **2012**, *50*, 835.
[31] H. Chen, M. B. Müller, K. J. Gilmore, G. G. Wallace, D. Li, *Adv. Mater.* **2008**, *20*, 3557.
[32] M. Lian, J. Fan, Z. Shi, S. Zhang, H. Li, J. Yin, *Carbon* **2015**, *89*, 279.
[33] M. Niño, J. M. R. Patino, *J. Am. Oil Chem. Soc.* **1998**, *75*, 1241.
[34] C. J. Shih, S. Lin, M. S. Strano, D. Blankschtein, *J. Am. Chem. Soc.* **2010**, *132*, 14638.
[35] L. Feng, Z. Liu, *Nanomedicine* **2011**, *6*, 317.
[36] A. Pattammattel, C. L. Williams, P. Pande, W. G. Tsui, A. K. Basu, C. V. Kumar, *R. Soc. Chem. Adv.* **2015**, *5*, 59364.
[37] S. Tenzer, D. Docter, J. Kuharev, A. Musyanovych, V. Fetz, R. Hecht, F. Schlenk, D. Fischer, K. Kiouptsi, C. Reinhardt, K. Landfester, H. Schild, M. Maskos, S. K. Knauer, R. H. Stauber, *Nat. Nanotechnol.* **2013**, *8*, 772.
[38] M. P. Monopoli, D. Walczyk, A. Campbell, G. Elia, I. Lynch, F. Baldelli Bombelli, K. A. Dawson, *J. Am. Chem. Soc.* **2011**, *133*, 2525.
[39] A. Pattammattel, M. Puglia, S. Chakraborty, I. K. Deshapriya, P. K. Dutta, C. V. Kumar, *Langmuir* **2013**, *29*, 15643.
[40] L. Vicarelli, S. J. Heerema, C. Dekker, H. W. Zandbergen, *ACS Nano* **2015**, *9*, 3428.

[41] Y. Q. Li, T. Yu, T. Y. Yang, L.-X. Zheng, K. Liao, *Adv. Mater.* **2012**, *24*, 3426.
[42] Q. Tang, Z. Zhou, Z. Chen, *Nanoscale* **2013**, *5*, 4541.
[43] A. C. Ferrari, F. Bonaccorso, V. Fal'ko, K. S. Novoselov, S. Roche, P. Boggild, S. Borini, F. H. L. Koppens, V. Palermo, N. Pugno, J. A. Garrido, R. Sordan, A. Bianco, L. Ballerini, M. Prato, E. Lidorikis, J. Kivioja, C. Marinelli, T. Ryhanen, A. Morpurgo, J. N. Coleman, V. Nicolosi, L. Colombo, A. Fert, M. Garcia-Hernandez, A. Bachtold, G. F. Schneider, F. Guinea, C. Dekker, M. Barbone, Z. Sun, C. Galiotis, A. N. Grigorenko, G. Konstantatos, A. Kis, M. Katsnelson, L. Vandersypen, A. Loiseau, V. Morandi, D. Neumaier, E. Treossi, V. Pellegrini, M. Polini, A. Tredicucci, G. M. Williams, B. Hee Hong, J.-H. Ahn, J. Min Kim, H. Zirath, B. J. van Wees, H. van der Zant, L. Occhipinti, A. Di Matteo, I. A. Kinloch, T. Seyller, E. Quesnel, X. Feng, K. Teo, N. Rupesinghe, P. Hakonen, S. R. T. Neil, Q. Tannock, T. Lofwander, J. Kinaret, *Nanoscale* **2015**, *7*, 4598.